The Astrophysical Journal, 743:131 (13pp), 2011 December 20 doi:10.1088/0004-637X/743/2/131

ON THE FORMATION OF INTERSTELLAR WATER ICE: CONSTRAINTS FROM A SEARCH FOR HYDROGEN PEROXIDE ICE IN MOLECULAR CLOUDS

R. G. Smith[1], S. B. Charnley[2], Y. J. Pendleton[3], C. M. Wright[1], M. M. Maldoni[4], and G. Robinson[1]
[1] School of Physical, Environmental & Mathematical Sciences, The University of New South Wales, Australian Defence Force Academy, Canberra, ACT 2600, Australia; r.smith@adfa.edu.au, c.wright@adfa.edu.au, g.robinson@adfa.edu.au
[2] Astrochemistry Laboratory, NASA Goddard Space Flight Center, Greenbelt, MD 20771, USA; Steven.B.Charnley@nasa.gov
[3] NASA Lunar Science Institute, NASA Ames Research Center, Moffett Field, CA 94035, USA; yvonne.pendleton@nasa.gov
[4] Geoscience Australia, Canberra, ACT 2601, Australia
Received 2011 January 31; accepted 2011 September 13; published 2011 November 29

ABSTRACT

Recent surface chemistry experiments have shown that the hydrogenation of molecular oxygen on interstellar dust grains is a plausible formation mechanism, via hydrogen peroxide (H_2O_2), for the production of water (H_2O) ice mantles in the dense interstellar medium. Theoretical chemistry models also predict the formation of a significant abundance of H_2O_2 ice in grain mantles by this route. At their upper limits, the predicted and experimental abundances are sufficiently high that H_2O_2 should be detectable in molecular cloud ice spectra. To investigate this further, laboratory spectra have been obtained for H_2O_2/H_2O ice films between 2.5 and 200 μm, from 10 to 180 K, containing 3%, 30%, and 97% H_2O_2 ice. Integrated absorbances for all the absorption features in low-temperature H_2O_2 ice have been derived from these spectra. For identifying H_2O_2 ice, the key results are the presence of unique features near 3.5, 7.0, and 11.3 μm. Comparing the laboratory spectra with the spectra of a group of 24 protostars and field stars, all of which have strong H_2O ice absorption bands, no absorption features are found that can definitely be identified with H_2O_2 ice. In the absence of definite H_2O_2 features, the H_2O_2 abundance is constrained by its possible contribution to the weak absorption feature near 3.47 μm found on the long-wavelength wing of the 3 μm H_2O ice band. This gives an average upper limit for H_2O_2, as a percentage of H_2O, of 9% $\pm$ 4%. This is a strong constraint on parameters for surface chemistry experiments and dense cloud chemistry models.

Key words: infrared: ISM – ISM: abundances – ISM: clouds – ISM: lines and bands – ISM: molecules – molecular processes

Online-only material: machine-readable tables

1. INTRODUCTION

An important problem in astrochemistry is identifying the formation mechanism for the interstellar water (H_2O) ice that coats the dust (e.g., van Dishoeck 2004) and constitutes a significant fraction of the oxygen budget in molecular clouds (Whittet 2010). Although production in gas-phase chemical reactions followed by condensation onto dust grains is possible (Bergin et al. 1999), the observational evidence strongly favors formation through chemical reactions on the surfaces of cold dust grains.

Three grain-surface pathways to H_2O ice have been proposed, each of which have now been studied in the laboratory using modern surface science techniques (e.g., Watanabe & Kouchi 2008). First, given the high abundances of O and H atoms available in molecular clouds, large amounts of H_2O ice could be produced following the addition of two hydrogen atoms to an accreted oxygen atom (e.g., Watson & Salpeter 1972; Watson 1976):

$$\mathrm{O} \xrightarrow{\mathrm{H}} \mathrm{OH} \xrightarrow{\mathrm{H}} \mathrm{H_2O}. \quad (1)$$

Tielens & Hagen (1982) proposed two additional pathways to H_2O ice formation, one via the hydrogenation of ozone (O_3),

$$\mathrm{O_3} \xrightarrow{\mathrm{H}} \mathrm{O_2} + \mathrm{OH} \quad (2a)$$

$$\mathrm{OH} + \mathrm{H_2} \longrightarrow \mathrm{H_2O} + \mathrm{H} \quad (2b)$$

and one via the hydrogenation of molecular oxygen (O_2),

$$\mathrm{O_2} \xrightarrow{\mathrm{H}} \mathrm{HO_2} \xrightarrow{\mathrm{H}} \mathrm{H_2O_2} \xrightarrow{\mathrm{H}} \mathrm{H_2O} + \mathrm{OH}. \quad (3)$$

Theoretical models of these pathways have shown that each could contribute to H_2O ice formation, depending on the cloud physical conditions (e.g., Tielens & Hagen 1982; Brown 1990; Hasegawa et al. 1992; Cuppen & Herbst 2007). For example, Tielens & Hagen (1982) argue that in pathway (3) quantum tunneling of hydrogen atoms through the relevant activation energy barriers should produce predominately H_2O ice mantles at densities $n_H < 10^5$ cm^{-3} and mostly O_2 at higher densities.

Pathway (1) has recently been demonstrated in the laboratory by Dulieu et al. (2010). Laboratory support for pathway (2) comes from the surface chemistry experiments of Mokrane et al. (2009) which have confirmed that H additions to O_3 can form water molecules. However, as O_3 is assumed to form by O atom addition to O_2, this is likely to be only a minor route to H_2O ice in realistic grain mantles since O_3 production is probably not competitive with the reactions in pathway (1) for oxygen atoms (Cuppen et al. 2010). Water production from solid O_2 via pathway (3), where the product OH radical can also be hydrogenated to H_2O, has also been demonstrated in the laboratory experiments of Miyauchi et al. (2008) and Ioppolo et al. (2008), although these experiments produced much more H_2O_2 than H_2O. However, more recent measurements by Oba et al. (2009) have shown that this pathway can produce ices with an H_2O_2 abundance as low as 20% relative to H_2O and they speculate that even lower H_2O_2 abundances (~3%), and

Table 1
Typical Initial Sample Solution and Final Ice Film (Distillate) Concentrations, by Percentage Mass of H_2O_2 and Molar Ratio, for the H_2O_2/H_2O Mixtures Used to Produce the Near- and Far-infrared H_2O_2 Spectra

Initial Solution		Final Ice Film	
% Mass	Molar Ratio	% Mass	Molar Ratio
30.9	1/4.2	2.6	1/70
71.6	1.3/1	30.1	1/4.4
99.5	105/1	97.2	18/1

consequently higher H_2O abundances, might be possible in molecular clouds.

Thus, experiments and the theoretical models indicate that H_2O_2 should always comprise at least a few percent of the mantle. Hence, there are reasonable grounds for expecting H_2O_2 in molecular cloud ices and the determination of its abundance relative to H_2O could provide a powerful constraint on the formation pathway to H_2O ice. This paper describes a search for H_2O_2 in astronomical ice absorption spectra, backed up by a laboratory study of H_2O_2 ice.

High-quality laboratory spectra for comparison with observations are essential for investigating the presence of H_2O_2 in molecular cloud ices. However, much of the earlier laboratory infrared spectroscopy of solid H_2O_2 and H_2O_2 mixtures (e.g., Taylor 1950; Giguère & Harvey 1959; Miller & Hornig 1961; Lannon et al. 1971) was primarily aimed at understanding the H_2O_2 structure and was measured at only a limited number of temperatures. Boudin et al. (1998) were the first to carry out a laboratory study of H_2O_2 as a possible component of molecular cloud ices, determining an upper limit of 5.2% for H_2O_2 relative to H_2O in NGC 7538/IRS 9. They presented spectra from 2.5 to 20 μm (4000–500 cm^{-1}) of H_2O_2/H_2O mixtures and made a limited exploration of the potential effects of thermal processing by comparing the position and FWHM of the absorption features on their spectra at 10, 80, and 120 K. There is good observational evidence for thermal processing of molecular cloud ices (e.g., Smith et al. 1989; Ehrenfreund et al. 1998; Boogert et al. 2000) and this may in fact be the dominant process as one moves from cold clouds to protostellar environments, so it is important to understand its effects.

This paper is organized as follows. We first present the results of a series of laboratory experiments measuring the near- and far-infrared spectra of H_2O_2/H_2O ice mixtures initially formed at 10 K and then as they were warmed up to the point where they began to evaporate. Our aim is to identify spectral features unique to H_2O_2 and to examine the effects of (1) varying the concentration of H_2O_2 and (2) thermal processing on the strengths and positions of these features. The temperature range for these measurements, 10–180 K, covers temperatures typical of molecular cloud ices. As far as we are aware, this is the first study of the far-infrared spectrum of H_2O_2 ice. Our results are complemented by existing measurements of pure H_2O ice made with the same apparatus over the same temperature and wavelength ranges by Smith et al. (1994) and Maldoni et al. (1998). The laboratory spectra are used to derive the integrated absorbances for all the major near- and far-infrared (up to 200 μm) H_2O_2 absorption features. In order to establish the existence of H_2O_2, or to place upper limits on its abundance, we then make a comparison between our laboratory spectra and the observed spectra of a number of bright infrared sources either embedded in or lying behind molecular clouds. Finally, we discuss the implications of our results in the light of current surface chemistry experiments and astrochemical models.

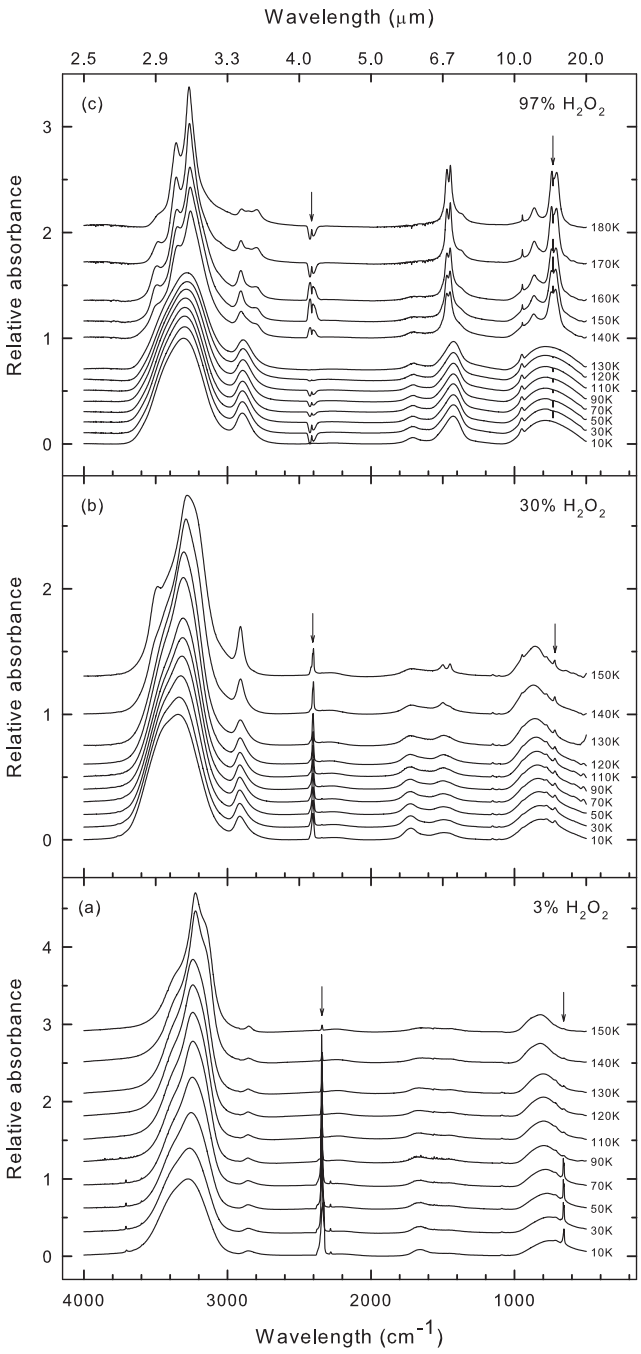

Figure 1. Near-infrared laboratory spectra of three H_2O_2/H_2O ice films with the mass concentrations shown in each panel. The films were initially deposited at 10 K and then slowly warmed up in the temperature steps shown until they began to evaporate. The bottom spectrum in each panel is the initial 10 K film and all the spectra in that panel have been normalized by the peak absorbance of this spectrum. Spectra above 10 K have been shifted vertically by an arbitrary amount to facilitate the display of the entire series. The arrows indicate spurious features caused by incomplete cancellation of the background or residual trapped gasses (see the text).

2. RESULTS

2.1. Laboratory Materials and Methods

The laboratory setup used to make the infrared spectral measurements of thin H_2O_2/H_2O ice films has already been described by Smith et al. (1994) and Maldoni et al. (1998). The methodology used by these authors has been followed, except for some details of the process used to form the ice films,

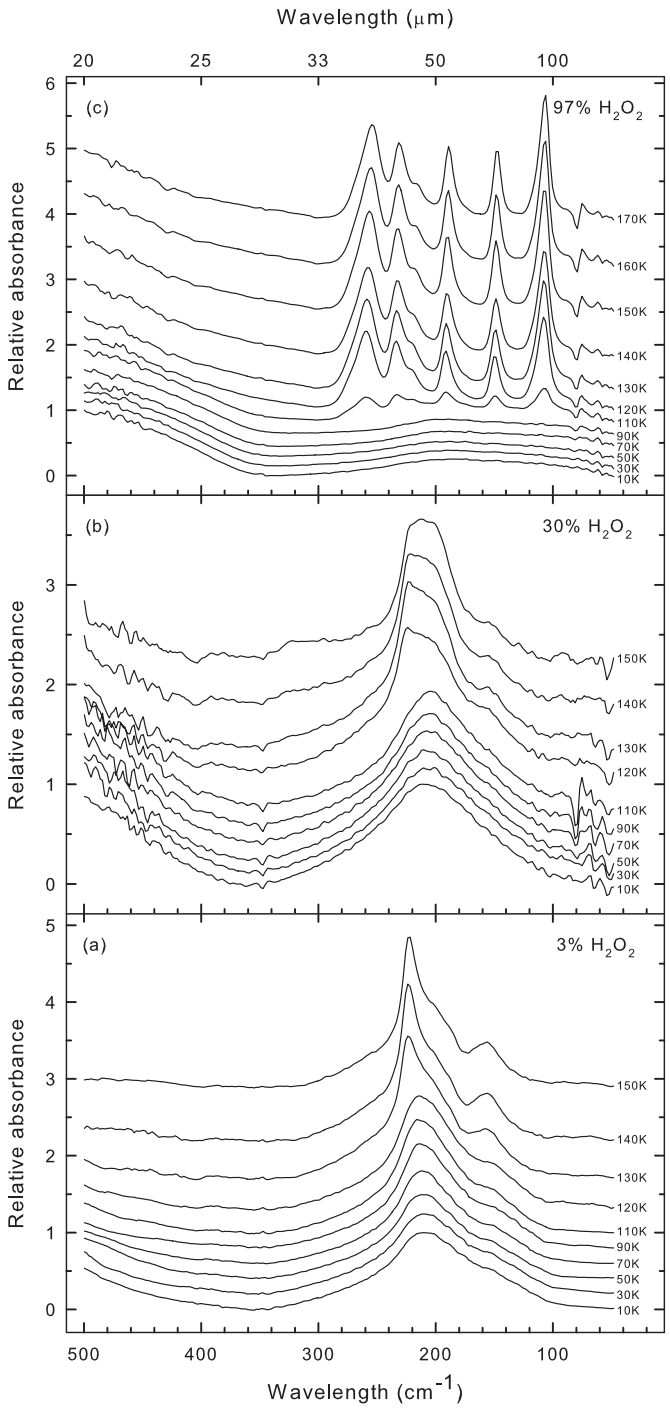

Figure 2. Far-infrared laboratory spectra of three H_2O_2/H_2O ice films with the mass concentrations shown in each panel. The films were initially deposited at 10 K and then slowly warmed up in the temperature steps shown until they began to evaporate. The bottom spectrum in each panel is the initial 10 K film and all the spectra in that panel have been normalized by the peak absorbance of this spectrum. Spectra above 10 K have been shifted vertically by an arbitrary amount to facilitate the display of the entire series.

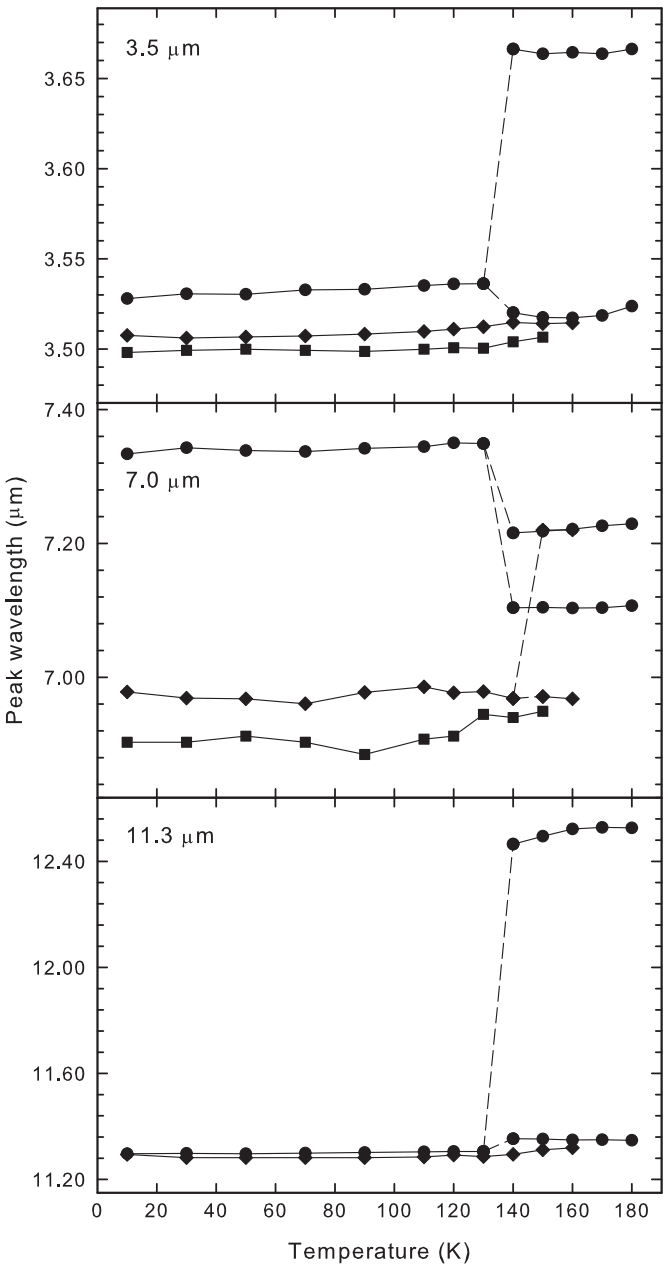

Figure 3. Effect of thermal processing on the peak wavelength of the 3.5, 7.0, and 11.3 μm H_2O_2 ice features. The three different H_2O_2 concentrations, 3%, 30%, and 97%, are represented by filled squares, filled diamonds, and filled circles, respectively. There are no data for the 11.3 μm feature from the 3% H_2O_2 spectra because it is not detectable at this concentration.

which are described below. For the near-infrared 2.5–25 μm (4000–400 cm^{-1}) measurements, H_2O_2/H_2O solutions were introduced into an evacuated sample chamber which contained a CsI substrate cooled to 10 K by a closed-cycle helium refrigerator and positioned so that the infrared transmission spectrum of the substrate and any ice film deposited on it could be measured with a Nicolet 740 Fourier transform infrared (FTIR) spectrometer. For the far-infrared 20–200 μm (500–50 cm^{-1}) measurements, the substrate was low-density polyethylene and the measurements were made with a model 20F optical bench attached to the Nicolet spectrometer. In each case the sample chamber windows were of the same material as the substrate. The spectral resolution was 4 cm^{-1} and each spectrum, including the background, comprised an average of 1024 spectrometer scans.

To form the ice films, a few drops of the sample solution were placed in a glass vessel attached to the sample chamber and frozen using liquid nitrogen. The sample chamber and the glass vessel were then evacuated and at least one thaw–freeze cycle under vacuum was carried out to remove any residual trapped gases. The substrate was subsequently cooled to 10 K.

Table 2
Absorbance Data for the 3% Near-infrared 2.5–25 μm (4000–400 cm^{-1}) H_2O_2/H_2O Ice Films

Wavelength (cm^{-1})	10 K	30 K	50 K	70 K	90 K	110 K	120 K	130 K	140 K	150 K
4.3594E+02	4.661E−03	5.283E−03	4.341E−03	4.686E−03	1.700E−02	5.572E−04	2.961E−03	4.245E−03	5.091E−03	6.933E−03
4.3797E+02	4.507E−03	5.194E−03	4.116E−03	4.276E−03	1.532E−02	9.295E−05	2.772E−03	3.822E−03	4.739E−03	6.248E−03
4.3980E+02	4.511E−03	5.024E−03	3.810E−03	3.912E−03	1.368E−02	−1.274E−04	2.440E−03	3.474E−03	4.326E−03	5.622E−03
4.4173E+02	4.491E−03	4.862E−03	3.591E−03	3.675E−03	1.241E−02	−1.704E−04	2.168E−03	3.174E−03	3.985E−03	5.003E−03
4.4366E+02	4.530E−03	4.620E−03	3.355E−03	3.323E−03	1.110E−02	−3.508E−04	1.873E−03	2.737E−03	3.508E−03	4.445E−03

(This table is available in its entirety in a machine-readable form in the online journal. A portion is shown here for guidance regarding its form and content.)

The sample was then allowed to thaw for a pre-determined period of time during which an ice film was gradually built up on the cold substrate. To maintain the integrity of the peroxide component while the ice film was forming, it was necessary to ensure that the H_2O_2 solutions only came into contact with glass surfaces up to the point where they entered the sample chamber. Note that this method of forming a mixed H_2O_2/H_2O ice film is different to that of Boudin et al. (1998) who produced their mixed films by simultaneous deposition of the subject and diluting gas through separate deposition tubes.

The H_2O_2 samples were purchased as 30% by mass solutions of H_2O_2 in H_2O (Riedel-deHaën, 30% extra pure) and this was the concentration used for our first ice film measurements. The concentration of this solution was subsequently increased by trap-to-trap distillation and shaking under reduced pressure ($\sim 10^{-1}$ torr) to first 70% and then 99.5% H_2O_2 by mass. At each stage the concentration was checked by acidic permanganate titration of a small portion of the sample solution. However, these concentrations are not the actual concentrations of the ice films that were ultimately measured. Because each ice film was formed by evaporation, the process of film formation is essentially one of distillation, thus the film will end up with a higher concentration of H_2O relative to H_2O_2 than the initial solution, by virtue of the higher volatility of H_2O. In view of the obvious difficulty in measuring the concentrations of the ice films directly, we reproduced the film formation process in the laboratory by distilling 30%, 70%, and 99% H_2O_2 solutions into glass flasks at 77 K and then measured the concentration of the distillate. Typical results are listed in Table 1. Also included in Table 1 are the concentrations expressed as molar ratios to facilitate comparison with the work of Boudin et al. (1998).

2.2. Laboratory Spectra

Near-infrared 2.5–25 μm (4000–400 cm^{-1}) and far-infrared 20–200 μm (500–50 cm^{-1}) spectra were measured for thin H_2O_2/H_2O ice films with estimated final H_2O_2 concentrations of 3%, 30%, and 97%. The ice films were first deposited at 10 K and then warmed up in 20 K steps below 110 K, and in 10 K steps above 110 K, until the film began to evaporate from the substrate. The warm-up was done slowly, typically allowing 30 minutes for a 10 K temperature change, to avoid any sudden energy input that might prematurely trigger a phase transition in the ice. These spectra are presented in Figures 1 and 2, respectively, and the raw data on which they are based are presented in Tables 2–7. The raw data are in units of absorbance, A_ν, where $A_\nu = \log_{10}(I_0/I)$, I_0 is the background intensity (before an ice film is deposited) and I is the intensity after an ice film is deposited. The wavelengths of all the absorption features in these spectra are listed in Table 8.

There are features in the spectra of Figure 1 near 4.3 and 15.2 μm due to carbon dioxide (CO_2). In the case of the 97% spectra, the features are due to gas-phase CO_2 and result from incomplete cancellation of the background, so they do not affect the observed ice spectra. However, in the case of the 30% and 3% spectra the features could also indicate the presence of CO_2 within the ice film, not completely removed by our initial freeze–thaw cycle. Because this could potentially affect the observed spectral features, we have estimated an upper limit for the concentration of CO_2 with respect to H_2O in these ice films. The CO_2 abundance was estimated using the strength of the 4.3 μm feature along with the integrated absorbance of the CO stretching vibration of CO_2 in H_2O (d'Hendecourt 1984). The H_2O abundance was estimated using the strength of the 3.08 μm feature corrected for the H_2O_2 contribution along with the integrated absorbances determined in Section 2.3 below. The resulting CO_2 concentration upper limits are 4% for the 30% H_2O_2 ice and 18% for the 3% H_2O_2 ice.

For identifying H_2O_2 ice in molecular cloud spectra, the key results from Figures 1 and 2 are the presence of features near 3.5, 7.0, and 11.3 μm unique to H_2O_2 ice in the spectra below $\sim$130 K. However, the strength of these features depends on the H_2O_2 concentration; at low concentrations (3%), the 3.5 μm feature is strong, the 7.0 μm feature is very weak, and the 11.3 μm feature is not detectable. At high concentrations (97%), the 7.0 μm feature is stronger than the 3.5 μm feature.

The effect of thermal processing on the peak wavelength and FWHM of these features is shown in Figures 3 and 4. The peak wavelengths are relatively constant for amorphous ice. Even after the amorphous–crystalline phase transition near 130 K, although the features are split and the wavelengths have changed, the peak wavelengths are still relatively constant (the largest wavelength shift is only 0.5%). Except for the 3.5 μm 97% feature, the FWHM of all the features decreases with increasing temperature.

Other important features of the spectra are summarized below.

1. As might be expected, the 3% H_2O_2 ice closely follows the behavior and appearance of pure H_2O ice (Smith et al. 1994; Maldoni et al. 1998), including the amorphous to crystalline phase transition near 110–120 K. The presence of H_2O_2 is marked by absorption features at 3.5 μm and 7.0 μm not present in H_2O ice.
2. 30% H_2O_2 ice again follows the behavior and appearance of pure H_2O ice except that a new feature unique to H_2O_2 appears near 11.3 μm in addition to the 3.5 μm and 7.0 μm features.
3. There are no distinct new far-infrared features in 30% H_2O_2 ice above the phase transition temperature, but the FWHM of the 48 μm feature is significantly broader than the equivalent H_2O ice feature.

Table 3
Absorbance Data for the 30% Near-infrared 2.5–25 μm (4000–400 cm^{-1}) H_2O_2/H_2O Ice Films

Wavelength (cm^{-1})	10 K	30 K	50 K	70 K	90 K	110 K	120 K	130 K	140 K	150 K	160 K
4.3594E+02	3.741E−03	3.962E−03	4.426E−03	−5.397E−03	−3.790E−03	−1.706E−03	−3.345E−03	2.930E−02	1.634E−03	8.798E−03	2.505E−02
4.3797E+02	3.818E−03	4.128E−03	4.521E−03	−3.793E−03	−2.342E−03	−5.991E−04	−2.646E−03	2.644E−02	1.401E−03	7.446E−03	2.295E−02
4.3980E+02	4.030E−03	4.433E−03	4.524E−03	−2.241E−03	−7.668E−04	5.688E−04	−1.915E−03	2.380E−02	1.094E−03	6.063E−03	2.067E−02
4.4173E+02	4.224E−03	4.652E−03	4.571E−03	−6.943E−04	7.962E−04	1.961E−03	−1.073E−03	2.154E−02	7.240E−04	4.901E−03	1.846E−02
4.4366E+02	4.575E−03	5.018E−03	4.776E−03	9.906E−04	2.237E−03	3.433E−03	−1.746E−04	1.968E−02	4.885E−04	3.689E−03	1.641E−02

(This table is available in its entirety in a machine-readable form in the online journal. A portion is shown here for guidance regarding its form and content.)

Table 4
Absorbance Data for the 97% Near-infrared 2.5–25 μm (4000–400 cm^{-1}) H_2O_2/H_2O Ice Films

Wavelength (cm^{-1})	10 K	30 K	50 K	70 K	90 K	110 K	120 K	130 K	140 K	150 K	160 K	170 K	180 K
4.3594E+02	1.276E−02	1.687E−02	1.780E−02	1.681E−02	1.484E−02	1.619E−02	1.850E−02	1.649E−02	5.924E−03	8.122E−03	9.008E−03	3.840E−03	7.773E−05
4.3797E+02	1.278E−02	1.625E−02	1.671E−02	1.539E−02	1.433E−02	1.542E−02	1.732E−02	1.549E−02	4.569E−03	6.623E−03	7.157E−03	2.676E−03	−6.469E−04
4.3980E+02	1.305E−02	1.559E−02	1.600E−02	1.510E−02	1.443E−02	1.513E−02	1.665E−02	1.515E−02	3.319E−03	5.215E−03	5.982E−03	2.298E−03	−1.142E−03
4.4173E+02	1.345E−02	1.540E−02	1.593E−02	1.473E−02	1.448E−02	1.573E−02	1.638E−02	1.494E−02	2.328E−03	4.361E−03	4.689E−03	1.593E−03	−1.773E−03
4.4366E+02	1.445E−02	1.543E−02	1.578E−02	1.490E−02	1.490E−02	1.621E−02	1.629E−02	1.485E−02	2.065E−03	3.541E−03	3.957E−03	1.072E−03	−2.203E−03

(This table is available in its entirety in a machine-readable form in the online journal. A portion is shown here for guidance regarding its form and content.)

Table 5
Absorbance Data for the 3% Far-infrared 20–200 μm (500–50 cm^{-1}) H_2O_2/H_2O Ice Films

Wavelength (cm^{-1})	10 K	30 K	50 K	70 K	90 K	110 K	120 K	130 K	140 K	150 K
4.822E+01	1.086E−03	1.111E−03	1.134E−03	4.670E−05	−1.216E−04	−1.841E−04	2.228E−03	1.168E−03	5.604E−04	6.443E−04
5.015E+01	8.695E−04	8.695E−04	8.695E−04	−4.279E−09	−2.095E−09	−3.095E−09	1.305E−03	1.305E−03	−3.356E−09	−3.848E−09
5.208E+01	9.365E−04	9.591E−04	1.167E−03	−1.432E−04	1.812E−04	−2.668E−06	2.540E−03	1.864E−03	1.662E−06	3.089E−04
5.401E+01	1.178E−03	1.006E−03	1.310E−03	−1.230E−05	4.977E−04	1.113E−04	3.731E−03	2.178E−03	7.809E−04	9.572E−04
5.594E+01	1.552E−03	1.271E−03	9.436E−04	−1.848E−04	7.834E−04	3.081E−04	4.323E−03	2.961E−03	9.649E−04	1.699E−03

(This table is available in its entirety in a machine-readable form in the online journal. A portion is shown here for guidance regarding its form and content.)

Table 6
Absorbance Data for the 30% Far-infrared 20–200 μm (500–50 cm^{-1}) H_2O_2/H_2O Ice Films

Wavelength (cm^{-1})	10 K	30 K	50 K	70 K	90 K	110 K	120 K	130 K	140 K	150 K
4.822E+01	−1.850E−03	1.914E−04	1.741E−04	1.646E−04	1.871E−04	2.028E−04	−1.967E−03	1.850E−04	1.534E−04	−2.040E−03
5.015E+01	−2.166E−03	−3.520E−03	−4.367E−03	−4.319E−03	−3.084E−03	−2.370E−04	−8.176E−03	−6.752E−04	−2.765E−03	−8.491E−03
5.208E+01	−6.403E−03	−3.314E−03	−7.251E−03	−6.730E−03	−3.152E−03	−3.467E−03	−9.629E−03	−5.638E−03	−5.688E−03	−1.231E−02
5.401E+01	−7.151E−03	−1.700E−03	−4.276E−03	−5.343E−03	−2.527E−03	−2.946E−03	−7.790E−03	−6.540E−03	−4.889E−03	−1.547E−02
5.594E+01	−2.245E−03	4.979E−03	2.016E−03	9.075E−04	3.685E−03	1.438E−03	−2.348E−03	7.387E−04	2.304E−03	−8.155E−03

(This table is available in its entirety in a machine-readable form in the online journal. A portion is shown here for guidance regarding its form and content.)

4. In 97% H_2O_2 ice the amorphous to crystalline phase transition occurs at a higher temperature (120–140 K) compared to the lower-concentration ices. The transition temperature is consistent with the work of Ghormley (1957; 140 K) and Hudson & Moore (2006; 125 K).
5. In 97% H_2O_2 ice, above the phase transition temperature, all of the features are split into two or more components. This splitting is consistent with the crystalline H_2O_2 ice model of Miller & Hornig (1961).
6. In 97% H_2O_2 ice, evaporation from the substrate occurs at higher temperatures compared to the lower-concentration ices, presumably reflecting the lower volatility of H_2O_2 compared to H_2O. The sublimation temperature of the H_2O_2 ice is 180–190 K.
7. The 6.08 μm feature in 97% H_2O_2 ice gradually disappears at high temperatures. Giguère & Harvey (1959) identify this feature with the H–O bending mode in H_2O, so its disappearance may signal the disappearance of H_2O from the H_2O_2/H_2O ice mixture.
8. Of the three features unique to H_2O_2 ice, the peak wavelength of the 7.0 μm feature shows the most significant shift toward longer wavelengths at high concentrations.

2.3. Integrated Absorbances

To estimate abundances the integrated absorbances (absolute intensities) for the H_2O_2 absorption features are needed. These were determined using the equation

$$A = \frac{1}{N}\int_{\nu_1}^{\nu_2} \tau d\nu \quad (4)$$

(Hudgins et al. 1993), where N is the column density of absorbing molecules in the beam (in molecules cm^{-2}), ν is the frequency (in cm^{-1}), and $\int_{\nu_1}^{\nu_2} \tau d\nu$ is the integrated band strength, τ being the optical depth. The resultant integrated absorbances (in cm molecule^{-1}) for 97% H_2O_2 ice at 10 K are listed in Table 9.

The column density of absorbers depends on the ice film thickness, but our laboratory setup is such that spectra and film thickness cannot be measured simultaneously, so a separate experiment was carried out to measure the film thickness. Two solid-state lasers were attached to the sample chamber and oriented so that they reflected off the sample substrate at different incidence angles. An ice film was then deposited on the substrate and the interference pattern between the laser light reflected from the substrate and the surface of the ice film was monitored. The two unknowns for the ice film are its thickness and its refractive index—with two interference patterns we can solve for both. This provided an estimate of the refractive index for 97% H_2O_2 ice at 10 K, 1.37 ± 0.05 at 670 nm, and allowed us to relate deposition time to film thickness. The column density also depends on the H_2O_2 ice density—we used 1.6 g cm^{-3} from Loeffler et al. (2006). Additionally, we assumed that the sample thickness is uniform over the area of the FTIR beam. There is also some uncertainty in the spectral baselines. Overall, this means there are very substantial uncertainties associated with the resultant integrated absorbances in Table 9, perhaps as high as 50%. However, a better idea of the true uncertainty can be obtained by comparison with published H_2O_2 ice integrated absorbances.

For the 3.5 μm feature the integrated absorbance in Table 9 of 1.6×10^{-17} compares reasonably with the value of 1.5×10^{-17} from Boudin et al. (1998) for their 4/1 H_2O_2/H_2O ice mixture (corresponding to a concentration of ∼90% by mass).

For the 7.33 μm feature, the integrated absorbance in Table 9 is a factor of 2.6 higher than the value of 7.0×10^{-18} from Boudin et al. (1998). However, the strength of the 7.33 μm feature (relative to the 3.5 μm feature) varies with H_2O_2 concentration; in our 97% H_2O_2 ice it is stronger than the 3.5 μm feature, and this is reflected in the integrated absorbances in Table 9. On the other hand, in the Boudin et al. (1998) H_2O_2 ice spectrum, the 7.33 μm feature is weaker than the 3.5 μm feature. Considering the trend in the relative strengths of these two features in our 3%, 30%, and 97% H_2O_2 ice spectra, the difference between the two absorbance values can be reconciled if the mass concentration of the Boudin et al. (1998) ice mixture was ∼80% rather than 90%.

Table 7
Absorbance Data for the 97% Far-infrared 20–200 μm (500–50 cm^{-1}) H_2O_2/H_2O Ice Films

Wavelength (cm^{-1})	10 K	30 K	50 K	70 K	90 K	110 K	120 K	130 K	140 K	150 K	160 K	170 K
4.822E+01	−3.161E−03	−7.777E−03	−4.750E−03	1.192E−0	−2.136E−03	−5.293E−03	−7.456E−03	−4.507E−03	−3.426E−03	−6.005E−03	−8.303E−03	−7.559E−03
5.015E+01	−2.138E−08	−2.192E−08	−2.263E−08	7.499E−03	−2.384E−08	1.305E−03	−1.854E−08	−1.803E−08	−1.550E−08	2.177E−03	−1.783E−08	−1.677E−08
5.208E+01	7.359E−04	−5.045E−04	−2.281E−03	5.143E−03	−8.068E−04	−1.362E−03	−1.088E−03	−1.698E−03	−3.698E−03	−1.859E−03	2.138E−03	−4.369E−04
5.401E+01	6.161E−03	2.127E−03	−6.825E−04	8.032E−03	3.075E−03	3.901E−03	2.836E−03	6.142E−03	−1.904E−03	1.286E−03	7.647E−03	3.339E−03
5.594E+01	5.027E−03	1.658E−03	−2.058E−03	7.677E−03	2.198E−03	3.435E−03	1.217E−03	6.659E−03	−9.401E−04	1.242E−03	5.857E−03	2.227E−03

(This table is available in its entirety in a machine-readable form in the online journal. A portion is shown here for guidance regarding its form and content.)

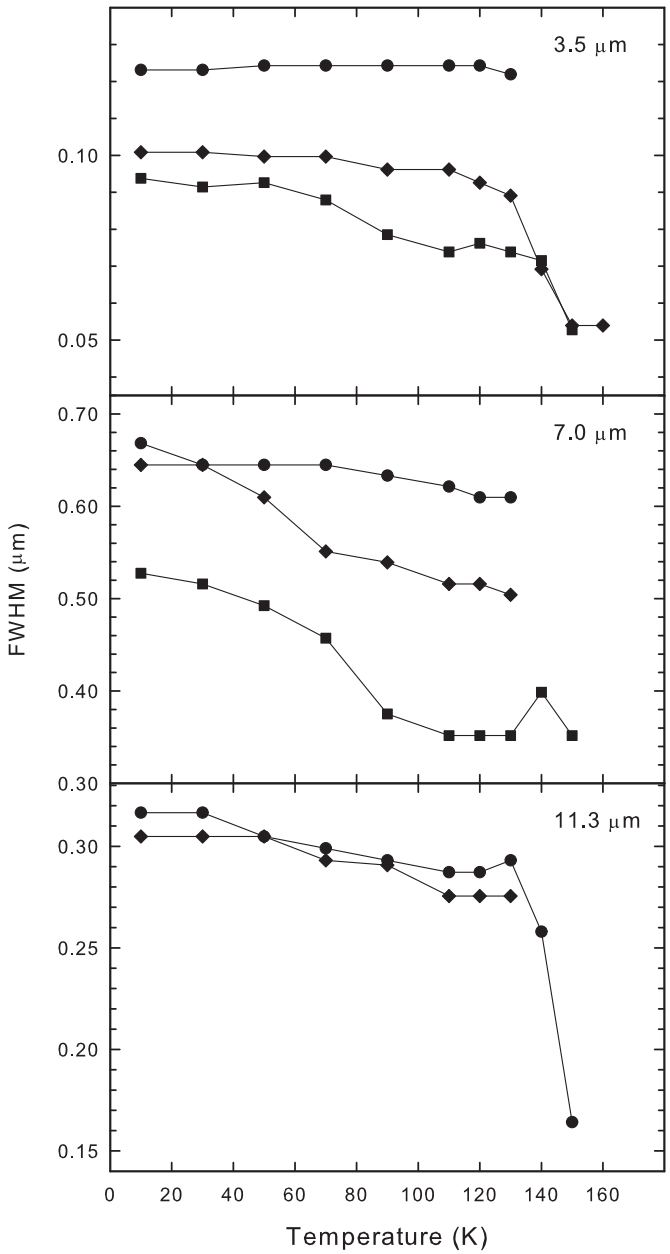

Figure 4. Effect of thermal processing on the FWHM of the 3.5, 7.0, and 11.3 μm H_2O_2 ice features. The three different H_2O_2 concentrations, 3%, 30%, and 97%, are represented by filled squares, filled diamonds, and filled circles, respectively. There are no data for the 11.3 μm feature from the 3% H_2O_2 spectra as it is not detectable at this concentration. The FWHM has not been plotted for the split features because the asymmetry of the split features makes determining a meaningful FWHM difficult.

Giguère & Harvey (1959) identify the 6.08 μm feature with the O–H bending mode in H_2O. This is consistent with the agreement between the integrated absorbance for this feature in Table 9 and the published values for the same band in H_2O ice: 8.4×10^{-18} (d'Hendecourt 1984) and 1×10^{-17} (Hudgins et al. 1993).

There is no published integrated absorbance for the strongest H_2O_2 feature, the 3.09 μm O–H stretching mode. However, the value in Table 9 compares reasonably with published values for the equivalent feature in H_2O ice, 2.0×10^{-16} (Hagen et al. 1981) and 1.7×10^{-16} (Hudgins et al. 1993), suggesting that both the H_2O_2 and H_2O O–H stretching modes have similar integrated absorbances. Given that both H_2O and H_2O_2 have

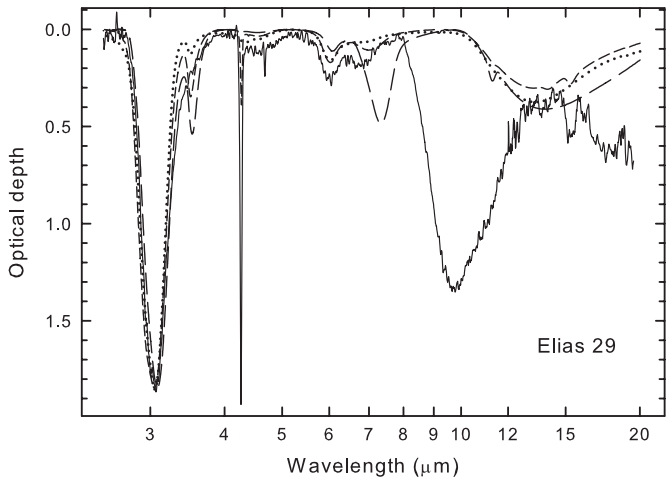

Figure 5. Comparison between the *ISO*-SWS spectrum of the protostar Elias 29 on an optical depth scale (solid line), and the laboratory absorbance spectra of 3%, 30%, and 97% H_2O_2 ice (dotted, short-dashed, and long-dashed lines, respectively) at 10 K, illustrating where H_2O_2 could contribute to the observed absorption.

similar hydrogen bond strengths (Miller & Hornig 1961) this is probably not unreasonable. What this means in practice, however, is that the optical depth of this feature can be used to give the combined column density of H_2O + H_2O_2 in any line of sight (see Section 2.4).

No attempt has been made to calculate the integrated absorbances for crystalline H_2O_2 because of the complex line splitting that takes place. However, the integrated band strengths of the crystalline 3.5 and 7.33 μm features, including the splitting, are comparable to the respective amorphous features to within ~15% so the integrated absorbances in Table 9 for these two features should generally be applicable to the crystalline features.

2.4. Comparison with Observations

In order to quantify the possible H_2O_2 component of molecular cloud ices, a group of low- and high-mass protostars and field stars lying behind molecular clouds were selected for comparison with the laboratory spectra (see Table 10). All of these sources are bright, well studied (i.e., most have published spectra covering all the wavelengths of interest), and have strong H_2O ice absorption bands. They have been divided into two groups on the basis of the appearance of the 3.08 μm H_2O ice absorption feature in their spectra which reflects different levels of thermal processing of the ice (see, e.g., the discussion in Smith et al. 1989). For protostars in the "unprocessed" group their 3.08 μm H_2O ice absorption features are typical of 10–20 K amorphous ice while the "processed" group have 3.08 μm features which are narrower and contain substructure consistent with exposure to higher temperatures.

To illustrate the potential contribution of H_2O_2 to the protostar and field-star spectra, one protostar, Elias 29 in the ρ Ophiuchus molecular cloud, is compared to the laboratory spectra of 3%, 30%, and 97% H_2O_2 ice in Figure 5. The Elias 29 spectrum is a plot of the *Infrared Space Observatory* (*ISO*) Short Wavelength Spectrometer (SWS) low-resolution pipeline processed and calibrated data described in Boogert et al. (2000). The data were converted to an optical depth scale using a continuum derived from a combination of blackbodies, reproducing as far as possible the Boogert et al. continuum; an exact match is not essential as no quantitative data are derived from this plot.

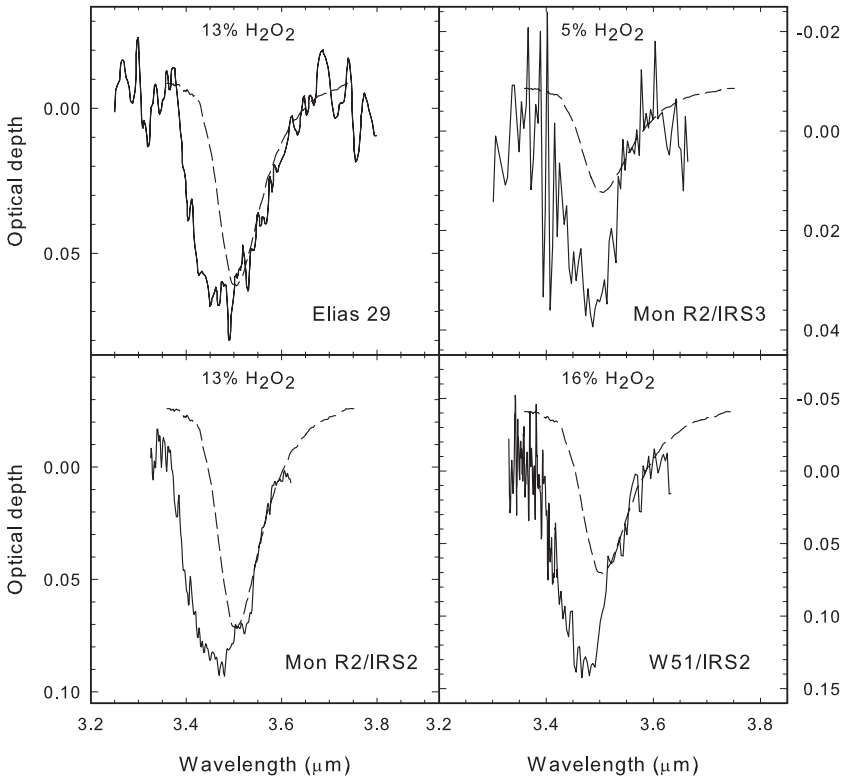

Figure 6. Baseline corrected 3.5 μm H_2O_2 feature from H_2O_2 ice at 10 K (dashed line) fitted to the 3.47 μm feature in Elias 29, Mon R2/IRS3, Mon R2/IRS2, and W51/IRS2. The 3.47 μm spectra are from Boogert et al. (2000; Elias 29), Sellgren et al. (1994; Mon R2/IRS3), and Brooke et al. (1999; Mon R2/IRS2 and W51/IRS2). Upper limits to the H_2O_2 abundance, as a percentage of H_2O, are shown for each source.

Inspecting the published spectra of Elias 29 in Figure 5 and the other protostars and field stars near 3.5, 7.0, and 11.3 μm, there are no absorption features in any of the spectra that can definitely be identified with H_2O_2 ice. There are, however, much broader absorptions that cover these wavelengths. For example, the 3.08 μm H_2O ice band has a long-wavelength wing that extends past 3.5 μm, the combination of absorption bands at 6.0 and 6.85 μm extends past 7.0 μm, and the normally strong silicate absorption extends past 11.3 μm as does the 12.2 μm H_2O librational band. Because of this underlying absorption, simply using the 3.5, 7.0, and 11.3 μm optical depths will not produce meaningful limits on the H_2O_2 abundance. There is, however, a weak absorption feature near 3.47 μm superimposed on the broad long-wavelength wing of the 3.08 μm ice band to which H_2O_2 could at least partially contribute. This feature is not obvious in Figure 5 because of its relative weakness compared to the long-wavelength wing. It extends from roughly 3.35 μm to 3.60 μm (see, e.g., Brooke et al. 1999) and is generally attributed to hydrocarbons (Allamandola et al. 1992; Pendleton 1997). Other identifications have, however, been proposed (e.g., ammonia hydrate; Dartois et al. 2002) and additional absorption attributed to CH_3OH (Grim et al. 1991) is seen in some objects near 3.54 μm.

To illustrate the possible contribution of H_2O_2 to the 3.47 μm feature, Figure 6 shows the profile of this feature on an optical depth scale for Elias 29 and three other objects from Table 10 (Mon R2/IRS3, Mon R2/IRS2, and W51/IRS2), compared to the laboratory profile of the 3.5 μm feature in 10 K H_2O_2 ice. The 3.47 μm spectra are from Boogert et al. (2000; Elias 29), Sellgren et al. (1994; Mon R2/IRS3), and Brooke et al. (1999; Mon R2/IRS2 and W51/IRS2). This does not necessarily mean that H_2O_2 is present in these or any of the other objects in Table 10, but it does illustrate why the optical depth at 3.5 μm provides a means of placing an upper limit to the amount of H_2O_2 that could be present.

At 7.0 μm there is no reliable way to separate out the contributions of the underlying 6.0 and 6.85 μm absorption features and the intrinsic weakness of the laboratory 11.3 μm feature makes it much less reliable for deriving upper limits than the other, stronger features. Hence we have not attempted to derive upper limits for these features.

To quantify the potential contribution of H_2O_2 to the protostar and field-star spectra, the optical depth, τ, can be converted to a column density, N, for the features of interest using the equation

$$N = \frac{\tau \Delta \nu}{A} \quad (5)$$

(d'Hendecourt 1984), where the integrated absorbance, A, is from Table 9 and $\Delta\nu$ is the FWHM of the feature.

The integrated absorbance at 3.08 μm is essentially the same for both H_2O_2 and H_2O, so the optical depth at this wavelength gives the column density of H_2O_2 + H_2O in the line of sight. Combining this with the optical depth at 3.50 μm within the 3.47 μm feature to derive the nominal column density of H_2O_2, the upper limits to the H_2O_2 abundance, relative to H_2O, were determined for all the objects in Table 10. For the entire group the H_2O_2 abundance ranges from 2% to 17%, with an average of 9% $\pm$ 4%. Within the uncertainties, there is no difference between the processed and unprocessed groups.

3. DISCUSSION

For low temperature ices and low H_2O_2 abundances there are only three spectral features, near 3.5, 7.0, and 11.3 μm,

Table 8
Laboratory Wavelengths (in μm) and Band Assignments of the Major Near-infrared Spectral Features of the Amorphous (10 K) and Crystalline (150 K) H_2O_2/H_2O Ice Mixtures Shown in Figures 1 and 2, Compared to Pure Amorphous (10 K) and Crystalline (140 K) H_2O Ice

Pure H_2O[a]	H_2O_2 Concentration			H_2O_2 Mode[b]
	3%	30%	97%	
Amorphous				
3.06	3.05	3.05	3.09	ν_1, ν_5: O–H stretch
...	3.50	3.51	3.53	$\nu_2 + \nu_6$, $2\nu_6$: H–O–O bend
4.53	4.53	4.56	4.54	$\nu_2 + \nu_7$ in H_2O
6.07	6.04	6.03	6.07	ν_2: H–O bend in H_2O
...	6.90	6.98	7.33	ν_6: H–O–O bend
...	...	11.29	11.30	ν_3: O-O stretch
13.44	13.29	13.27	13.85	ν_7: libration
46.51	47.62	47.39	48.31	Lattice
Crystalline				
...	...	2.92	2.92	
3.11	3.10	3.11	3.05	ν_1: O–H stretch
...	...		3.13	ν_5: O–H stretch
...	3.51	3.51	3.52	$\nu_2 + \nu_6$, $2\nu_6$: H–O–O bend
...	...		3.67	$2\nu_2$
4.46	4.46	4.51	...	$\nu_2 + \nu_7$ in H_2O
6.17	6.10	6.06	6.11	ν_2: H–O bend in H_2O
...	6.95	6.97	7.10	ν_2: H–O–O bend
...	...	7.22	7.22	ν_6: H–O–O bend
...	...	11.31	11.35	ν_3: O–O stretch
12.24	12.20	12.59	12.50	ν_7+ lattice
...	...	...	14.75	ν_4: torsion
...		...	15.38	ν_7: libration
...	...	...	38.91	Lattice
...	...	...	43.10	Lattice
44.44	45.05	46.95	45.87	Lattice
...	...	...	52.63	Lattice
63.69	64.10	65.79	67.57	Lattice
...	...	...	93.46	Lattice

Notes.
[a] From Maldoni et al. (1998).
[b] Using the notation of Giguère & Harvey (1959).

which distinguish H_2O_2 ice from H_2O ice. For high temperature ices (>130 K) and high H_2O_2 abundances, these features are split into at least two components and the differences between H_2O_2 and H_2O become more pronounced. Thermal processing has very little effect on their peak wavelengths, however the FWHM of all these features, except the 3.5 μm 97% feature, decrease with increasing temperature. Inspecting a sample of 24 molecular cloud ice spectra, there are no distinct H_2O_2 features apparent near 3.5, 7.0, and 11.3 μm, and so there is no conclusive evidence for H_2O_2 as a grain mantle constituent. However, there is a weak feature near 3.47 μm superimposed on the long-wavelength wing of the 3.08 μm O–H stretching feature to which H_2O_2 could at least partially contribute. Considering the maximum possible contribution of H_2O_2 to this feature for the entire sample of molecular cloud ice spectra, the upper limits to the H_2O_2 abundance relative to H_2O ice range from 2% to 17%, with an average of 9% ± 4%. The only other estimate of the H_2O_2 abundance in molecular cloud ices is from Boudin et al. (1998) who determined an upper limit of 5.2% for H_2O_2 relative to H_2O in NGC 7538/IRS 9. In contrast to the approach used here, Boudin et al. determined the H_2O abundance from the strength of the 6.08 μm feature in NGC 7538/IRS 9 rather than the 3.08 μm feature.

Table 9
Peak Wavelengths, Bandwidths (FWHM), and Integrated Absorbances for All the Observed Spectral Features in the Near- and Far-infrared Spectra of 97% H_2O_2 Ice at 10 K

Feature Wavelength		FWHM ($\Delta\nu$)	A
(μm)	(cm^{-1})	(cm^{-1})	(cm molecule $^{-1}$)
3.09	3241	350	2.0×10^{-16}
3.53	**2834**	**110**	$\mathbf{1.6 \times 10^{-17}}$
4.54	2205	325	2.1×10^{-18}
6.07	1647	95	1.0×10^{-17}
7.33	**1364**	**145**	$\mathbf{1.8 \times 10^{-17}}$
11.30	**885**	**25**	$\mathbf{6.0 \times 10^{-19}}$
13.85	722	350	4.2×10^{-17}
48.31	207	140	4.1×10^{-19}

Notes. The features unique to H_2O_2 are highlighted. The remaining H_2O_2 features are too close in wavelength to H_2O features to be distinguished.

The laboratory experiments of Oba et al. (2009) suggest that hydrogenation of O_2 may be the primary route to water production in grain mantles. Oba et al. demonstrated that at the low temperatures of molecular clouds, ices with an H_2O_2 abundance of ~20% relative to H_2O can be expected if the O_2/H flux ratio is $\sim 2 \times 10^{-3}$, and, by extrapolation, abundances of ~3% may be possible if $O_2/H \sim 2 \times 10^{-4}$. These abundances are consistent with our observed upper limits, but are the O_2/H flux ratios realistic in molecular clouds? Molecular oxygen has proven very difficult to detect in molecular clouds, with mostly only upper limits reported (e.g., Goldsmith et al. 2000). However, O_2 was detected by Larsson et al. (2007) in the ρ Oph A molecular cloud with an abundance of 5×10^{-8} relative to H_2. We take this as an upper limit to the O_2 number density in molecular clouds in the form $n(O_2) = 2.5 \times 10^{-8} n_H$. We assume that $n(H) = 1\,cm^{-3}$ is typical of the H atom concentration in molecular gas with $n_H \geqslant 2 \times 10^4\,cm^{-3}$ and that $n(H) = (5\text{–}27) \times 10^{-4} n_H$ is typical for gas at lower densities ($n_H < 10^4\,cm^{-3}$; Goldsmith & Li 2005). For the higher density gas the interstellar O_2/H flux ratios ($n(O_2)/n(H)$) corresponding to experimental values of $\sim 2 \times 10^{-3}$ and $\sim 2 \times 10^{-4}$ require interstellar gas densities of $n_H \sim 10^5\,cm^{-3}$ and $n_H \sim 10^4\,cm^{-3}$, respectively. For the lower density molecular gas the potentially higher (i.e., non-steady-state) H atom concentrations lead to density-independent O_2/H flux ratios of $\sim (0.9\text{–}5) \times 10^{-5}$. Thus, the requisite O_2/H flux ratios are possible in molecular clouds.

As this article was being revised, several papers have appeared which allow further insights into the proposed roles for O_2 and H_2O_2 in interstellar H_2O production. Gas-phase H_2O_2 has been discovered in the ρ Oph A molecular cloud by Bergman et al. (2011), where O_2 was previously detected (Larsson et al. 2007). The estimated H_2O_2 abundance relative to H_2 is about 10^{-10}, however, at present it is not possible to constrain the H_2O_2/H_2O ratio as the H_2O abundance in this source is not known. Goldsmith et al. (2011) have recently reported the detection of O_2 in Orion. The O_2 emission traces warm gas with temperatures in excess of about 150–180 K and is tentatively associated with the so-called Western Clump, adjacent to the Hot Core. This environment is more energetic than ρ Oph A and the high O_2 abundance ($O_2/H_2 = 1.3 \times 10^{-6}$) could be produced either by gas-phase chemistry following H_2O ice mantle evaporation, or in low-velocity shock waves (Goldsmith et al. 2011). Blake et al. (1987) previously reported an upper limit of $H_2O_2/H_2 < 4.5 \times 10^{-10}$ from a spectral line survey of Orion which included emission from the Western Clump.

Table 10
Upper Limits to the H_2O_2 Ice Abundances, Relative to H_2O Ice, for a Selection of Protostars and Field Stars Based on the Optical Depth at 3.50 μm Within the 3.47 μm Feature

Source	$\tau_{3.08}$	$\tau_{3.50}$	% H_2O_2	Ref
Unprocessed				
W3/IRS5	3.48	0.08	7	2,3
Tau/Elias 18	0.80	0.02	8	4,3
Tau/Elias 16	1.26	0.02	5	5,6
Mon R2/IRS2	2.54	0.10	13	2,7
S255/IRS 1	1.48	0.01	2	2,3
GL 961E	2.46	0.05	6	2,3
ρ Oph/Elias 29	1.85	0.07	13	9
ρ Oph/WL 6	2.1	0.05	8	10,7
ρ Oph/Elias 21	0.77	0.03	13	10,7
ρ Oph/Elias 33	1.00	0.02	6	10,7
RNO 91	2.1	0.08	13	7
Ser/SVS 20	1.0	0.03	10	12,7
RCrA/IRS 1	1.44	0.03	7	13,7
RCrA/IRS 2	1.1	0.03	9	14,7
RCrA/IRS 5	2.3	0.08	11	14,7
S140/IRS1	1.28	0.02	5	1,3
NGC7538/IRS1	1.29	0.03	7	1,3
NGC7538/IRS9	3.28	0.16	17	1,7
Processed				
Tau/HL Tau	0.77	0.01	4	5,6
BN	1.78	0.03	5	2,3
Mon R2/IRS3	1.14	0.02	5	2,8
AFGL 2136	3.2	0.15	16	11,7
AFGL 2591	0.92	0.04	15	2,7
W51/IRS2	2.4	0.11	16	7

References. (1) Willner et al. 1982; (2) Smith et al. 1989; (3) Brooke et al. 1996; (4) Whittet et al. 1988; (5) Sato et al. 1990; (6) Chiar et al. 1996; (7) Brooke et al. 1999; (8) Sellgren et al. 1994; (9) Boogert et al. 2000; (10) Tanaka et al. 1990; (11) Kastner & Weintraub 1996; (12) Eiroa & Hodapp 1989; (13) Whittet et al. 1996; (14) Tanaka et al. 1994.

Observations with *Herschel* show that H_2O is highly abundant and widespread in Orion (Melnick et al. 2010). Thus, adopting $H_2O/H_2 \sim 1 \times 10^{-5}$ as appropriate (Melnick et al. 2010), and assuming complete ice mantle evaporation has occurred,[5] we derive $O_2/H_2O = 13\%$ and $H_2O_2/H_2O < 0.0045\%$, the latter value being well within our limits.

4. CONCLUSIONS

A combination of laboratory measurements and comparison with astronomical spectra has allowed us to place limits on the abundance of solid hydrogen peroxide residing in interstellar ice mantles. Our derived limits are consistent with those expected from laboratory studies of water production from hydrogenation of solid O_2 and related observational data for gaseous H_2O_2 in two distinct environments.

What does this mean for interstellar H_2O formation from O_2? Interstellar molecular oxygen is rare (Goldsmith et al. 2000, 2011) but, irrespective of the problem of accounting for the unexpectedly low abundance of O_2, it is uncertain that solid H_2O abundances of a few times 10^{-5} (e.g., Whittet 1993) can be produced by freeze-out from such a low-abundance reservoir of gaseous O_2 over the relatively short lifetime of molecular clouds ($\sim$(0.25–1) $\times$ 10^6 yr; Hatchell et al. 2007; Enoch et al. 2008). This may suggest that the requisite O_2 should form on dust grains by recombination of two oxygen atoms (Tielens & Hagen 1982). However, although the calculated H_2O_2/H_2O mantle ratios of Tielens & Hagen are broadly within our limits, this must be considered fortuitous as this model contains several serious flaws concerning the treatment of the kinetics (leading to, for example, O_2 dominating the mantle composition) that, when corrected, do not lead to large O_2 abundances on grains by atom recombination (Charnley 2001, 2005; Charnley & Rodgers 2009). Nevertheless, if O_2 and H_2O_2 *are* involved in H_2O formation as proposed, one would expect they should be common molecules in hot cores and hot corinos, and so searches for them in such sources should be enlightening.

To conclude, the, albeit-limited, observational data now available for a possible chemical connection between O_2, H_2O_2, and H_2O present a significant challenge for gas-grain chemistry models in which H_2O ice is derived from O_2.

This work would not have been possible without the contribution of Vernon Edge who prepared all of the H_2O_2/H_2O samples and helped in numerous other ways with the experiments. C.M.W. acknowledges support from Australian Research Council Discovery Project DP0345227. S.B.C. acknowledges support from NASA's Exobiology and Evolutionary Biology Program.

[5] As it has a higher binding energy than H_2O (see Section 2.2), some H_2O_2 may remain on the dust and so the actual ratio in the original ices could be higher.

REFERENCES

Allamandola, L. J., Sandford, S. A., Tielens, A. G. G. M., & Herbst, T. M. 1992, ApJ, 399, 134
Bergin, E. A., Neufeld, D. A., & Melnick, G. J. 1999, ApJ, 510, L145
Bergman, P., Parise, B., Liseau, R., et al. 2011, A&A, 531, L8
Blake, G. A., Sutton, E. C., Masson, C. R., & Phillips, T. G. 1987, ApJ, 315, 621
Boogert, A. C. A., Tielens, A. G. G. M., Ceccarelli, C., et al. 2000, A&A, 360, 683
Boudin, N., Schutte, W. A., & Greenberg, J. M. 1998, A&A, 331, 749
Brooke, T. Y., Sellgren, K., & Geballe, T. R. 1999, ApJ, 517, 883
Brooke, T. Y., Sellgren, K., & Smith, R. G. 1996, ApJ, 459, 209
Brown, P. D. 1990, MNRAS, 243, 65
Charnley, S. B. 2001, ApJ, 562, L99
Charnley, S. B. 2005, Adv. Space Res., 36, 132
Charnley, S. B., & Rodgers, S. D. 2009, in ASP Conf. Ser. 40, Bioastronomy 2007: Molecules, Microbes and Extraterrestrial Life, ed. K. Meech et al. (San Francisco, CA: ASP), 29
Chiar, J. E., Adamson, A. J., & Whittet, D. C. B. 1996, ApJ, 472, 665
Cuppen, H. M., & Herbst, E. 2007, ApJ, 668, 294
Cuppen, H. M., Romanzin, C., van Dishoeck, E. F., & Linnartz, H. 2010, Phys. Chem. Chem. Phys., 12, 12077
Dartois, E., d'Hendecourt, L., Thi, W., Pontoppidan, K. M., & van Dishoeck, E. F. 2002, A&A, 394, 1057
d'Hendecourt, L. B. 1984, PhD thesis, Leiden Univ.
Dulieu, F., Amiaud, L., Congiu, E., et al. 2010, A&A, 512, A30
Ehrenfreund, P., Dartois, E., Demyk, K., & d'Hendecourt, L. 1998, A&A, 339, L17
Eiroa, C., & Hodapp, K.-W. 1989, A&A, 210, 345
Enoch, M. L., Evans, N. J., II, Sargent, A. I., et al. 2008, ApJ, 684, 1240
Ghormley, J. A. 1957, J. Am. Chem. Soc., 79, 1862
Giguère, P. A., & Harvey, K. B. 1959, J. Mol. Spectrosc., 3, 36
Goldsmith, P. F., & Li, D. 2005, ApJ, 622, 938
Goldsmith, P. F., Melnick, G. J., Bergin, E. A., et al. 2000, ApJ, 539, L123
Goldsmith, P. F., Liseau, R., & Bell, T. A. 2011, ApJ, 737, 96
Grim, R. J. A., Baas, F., Geballe, T. R., Greenberg, J. M., & Schutte, W. 1991, A&A, 247, 473
Hagen, W., Tielens, A. G. G. M., & Greenberg, J. M. 1981, Chem. Phys., 56, 367
Hasegawa, T. I., Herbst, E., & Leung, C. M. 1992, ApJS, 82, 167
Hatchell, J., Fuller, G. A., Richer, J. S., Harries, T. J., & Ladd, E. F. 2007, A&A, 468, 1009
Hudgins, D. M., Sandford, S. A., Allamandola, L. J., & Tielens, A. G. G. M. 1993, ApJS, 86, 713

Hudson, R. L., & Moore, M. H. 2006, Astrobiology, 6, 483
Ioppolo, S., Cuppen, H. M., Romanzin, C., van Dishoeck, E. F., & Linnarz, H. 2008, ApJ, 686, 1474
Kastner, J. H., & Weintraub, D. A. 1996, ApJ, 466, L103
Lannon, J. A., Verderame, F. D., & Anderson, R. W., Jr. 1971, J. Chem. Phys., 54, 2212
Larsson, B., Liseau, R., Pagani, L., et al. 2007, A&A, 466, 999
Loeffler, M. J., Raut, U., Vidal, R. A., Baragiola, R. A., & Carlson, R. W. 2006, Icarus, 180, 265
Maldoni, M. M., Smith, R. G., Robinson, G., & Rookyard, V. L. 1998, MNRAS, 298, 251
Melnick, G. J., Tolls, V., Neufeld, D. A., et al. 2010, A&A, 521, L27
Miller, R. L., & Hornig, D. F. 1961, J. Chem. Phys., 34, 265
Miyauchi, N., Hidaka, H., Chigai, T., et al. 2008, Chem. Phys. Lett., 456, 27
Mokrane, H., Chaabouni, H., Accolla, M., et al. 2009, ApJ, 705, L195
Oba, Y., Miyauchi, N., Hidaka, H., et al. 2009, ApJ, 701, 464
Pendleton, Y. J. 1997, Orig. Life Evol. Biosph., 27, 52
Sato, S., Nagata, T., Tanaka, M., & Yamamoto, T. 1990, ApJ, 359, 192
Sellgren, K., Smith, R. G., & Brooke, T. Y. 1994, ApJ, 433, 179
Smith, R. G., Robinson, G., Hyland, A. R., & Carpenter, G. L. 1994, MNRAS, 271, 481
Smith, R. G., Sellgren, K., & Tokunaga, A. T. 1989, ApJ, 344, 413
Tanaka, M., Nagata, T., Sato, S., & Yamamoto, T. 1994, ApJ, 430, 779
Tanaka, M., Sato, S., Nagata, T., & Yamamoto, T. 1990, ApJ, 352, 724
Taylor, R. C. 1950, J. Chem. Phys., 18, 898
Tielens, A. G. G. M., & Hagen, W. 1982, A&A, 114, 245
van Dishoeck, E. F. 2004, ARA&A, 42, 119
Watanabe, N., & Kouchi, A. 2008, Prog. Surf. Sci., 83, 439
Watson, W. D. 1976, Rev. Mod. Phys., 48, 513
Watson, W. D., & Salpeter, E. E. 1972, ApJ, 174, 321
Whittet, D. C. B. 1993, in Dust and Chemistry in Astronomy, ed. T. J. Millar & D. A. Williams (Bristol: IOP Publishing), 9
Whittet, D. C. B. 2010, ApJ, 710, 1009
Whittet, D. C. B., Bode, M. F., Longmore, A. J., et al. 1988, MNRAS, 233, 321
Whittet, D. C. B., Smith, R. G., Adamson, A. J., et al. 1996, ApJ, 458, 363
Willner, S. P., Gillett, F. C., Herter, T. L., et al. 1982, ApJ, 253, 174